

Specific penetration and accumulation of a homing peptide within atherosclerotic plaques of apolipoprotein E-deficient mice

Juliana Hamzah^a, Venkata R. Kotamraju^a, Jai W. Seo^b, Lilach Agemy^a, Valentina Fogal^{c,1}, Lisa M. Mahakian^b, David Peters^a, Lise Roth^a, M. Karen J. Gagnon^b, Katherine W. Ferrara^b, and Erkki Ruoslahti^{a,c,2}

^aVascular Biology Laboratory, Center for Nanomedicine, The Sanford-Burnham Medical Research Institute, Department of Molecular, Cellular, and Developmental Biology, University of California, Santa Barbara, CA 93106-9610; ^bDepartment of Biomedical Engineering, University of California, Davis, CA 95616; and ^cCancer Research Center, The Sanford-Burnham Institute for Medical Research, La Jolla, CA 92037

Contributed by Erkki Ruoslahti, March 22, 2011 (sent for review January 18, 2011)

The ability to selectively deliver compounds into atherosclerotic plaques would greatly benefit the detection and treatment of atherosclerotic disease. We describe such a delivery system based on a 9-amino acid cyclic peptide, LyP-1. LyP-1 was originally identified as a tumor-homing peptide that specifically recognizes tumor cells, tumor lymphatics, and tumor-associated macrophages. As the receptor for LyP-1, p32, is expressed in atherosclerotic plaques, we tested the ability of LyP-1 to home to plaques. Fluorescein-labeled LyP-1 was intravenously injected into apolipoprotein E (ApoE)-null mice that had been maintained on a high-fat diet to induce atherosclerosis. LyP-1 accumulated in the plaque interior, predominantly in macrophages. More than 60% of cells released from plaques were positive for LyP-1 fluorescence. Another plaque-homing peptide, CREKA, which binds to fibrin-fibronectin clots and accumulates at the surface of plaques, yielded fewer positive cells. Tissues that did not contain plaque yielded only traces of LyP-1⁺ cells. LyP-1 was capable of delivering intravenously injected nanoparticles to plaques; we observed abundant accumulation of LyP-1-coated superparamagnetic iron oxide nanoparticles in the plaque interior, whereas CREKA-nanoworms remained at the surface of the plaques. Intravenous injection of 4-[¹⁸F]fluorobenzoic acid ([¹⁸F]FBA)-conjugated LyP-1 showed a four- to sixfold increase in peak PET activity in aortas containing plaques (0.31% ID/g) compared with aortas from normal mice injected with [¹⁸F]FBA-LyP-1 (0.08% ID/g, $P < 0.01$) or aortas from atherosclerotic ApoE mice injected with [¹⁸F]FBA-labeled control peptide (0.05% ID/g, $P < 0.001$). These results indicate that LyP-1 is a promising agent for the targeting of atherosclerotic lesions.

cell-penetrating peptide | p32/gC1qR/hyaluronic acid binding protein1 | plaque-associated macrophages | in vivo imaging

The diagnosis and treatment of atherosclerosis is dominated by the detection of arterial occlusions, reversal of these occlusions by physical intervention, and long-term management of lipid metabolism. Much less effort has been directed to developing reagents that can specifically target the cellular and molecular components of atherosclerotic lesions. However, such reagents could be valuable in specifically delivering imaging agents and therapeutics directly into plaques. Targeted delivery that uses carrier molecules with specific affinity for the target tissue (synaptic targeting) increases the efficacy of the targeted drug, but also reduces side effects (1).

The inherent propensity of macrophages to take up nanoparticles has been used to image plaque (2), and an optical probe activated by proteolytic enzymes that are abundant in the plaque environment has been described (3). However, the tendency of nanoparticles to home in plaques is obscured by nonspecific uptake by phagocytes in other tissues, and redundancies in protease expression and specificity tend to limit the selectivity of protease-based approaches.

In vivo phage display (4) has been used with some success to identify reagents with improved specificity for plaque targeting (5–11). We have shown that the pentapeptide CREKA, which binds to fibrin-fibronectin complexes in clotted plasma (12), homes to plaques (10). Following intravenous injection, CREKA-conjugated micelles bound to the surface of plaques and predominantly concentrated at the shoulders of the plaque, which is a location that is prone to rupture (10). An antithrombotic agent incorporated into the CREKA micelles also accumulated in plaques to a greater extent than when incorporated into control micelles.

Atheroma-associated macrophages in plaques are a prime cell target because of their role in plaque development and their unique features that are not shared by normal tissue macrophages (13). Consequently, atheroma-associated macrophages may be a suitable synaptic target.

LyP-1, a cyclic, 9-amino acid tumor-homing peptide (sequence: CGNKRTRGC), accumulates in tumor macrophages (14, 15). The receptor for LyP-1 is a protein known as p32/gC1qR/HABP1 (14). This protein is a mitochondrial protein in normal cells, but its expression and subcellular location is altered in many human carcinomas and experimental tumors. In addition to general overexpression of p32 in tumors, p32 is present at the cell surface in tumor cells and stromal cells within tumors. Tumor macrophages and the luminal lining of tumor lymphatics are strongly positive for cell surface p32, and tumor-specific homing of intravenously injected LyP-1 peptide is based on the accumulation of LyP-1 in these cells (14). Atherosclerotic plaques contain p32, particularly in the macrophages and foam cells (16). We set out to study whether this plaque p32 would be a suitable receptor for plaque targeting with the LyP-1 peptide.

Results

Homing of LyP-1 Peptide to Atherosclerotic Plaques in Vivo. To detect peptide homing to plaques, we analyzed the distribution of intravenously injected peptides that had been labeled with 5(6)-carboxy fluorescein (FAM). Histology analyses of aortas revealed extensive accumulation of FAM-LyP-1 inside the plaque tissue (Fig. 1A). Staining with an antifluorescein antibody confirmed the presence of LyP-1 in the plaques. For comparison, we also injected mice with a peptide previously shown to home to

Author contributions: J.H. and E.R. designed research; J.H., V.R.K., J.W.S., L.A., V.F., L.M.M., D.P., L.R., and M.K.J.G. performed research; L.A. and K.W.F. contributed new reagents/analytic tools; J.H. and K.W.F. analyzed data; and J.H. and E.R. wrote the paper.

The authors declare no conflict of interest.

¹Present address: Moores Cancer Center, University of California at San Diego, La Jolla CA 92093.

²To whom correspondence should be addressed. E-mail: ruoslahti@sanfordburnham.org.

This article contains supporting information online at www.pnas.org/lookup/suppl/doi:10.1073/pnas.1104540108/-DCSupplemental.

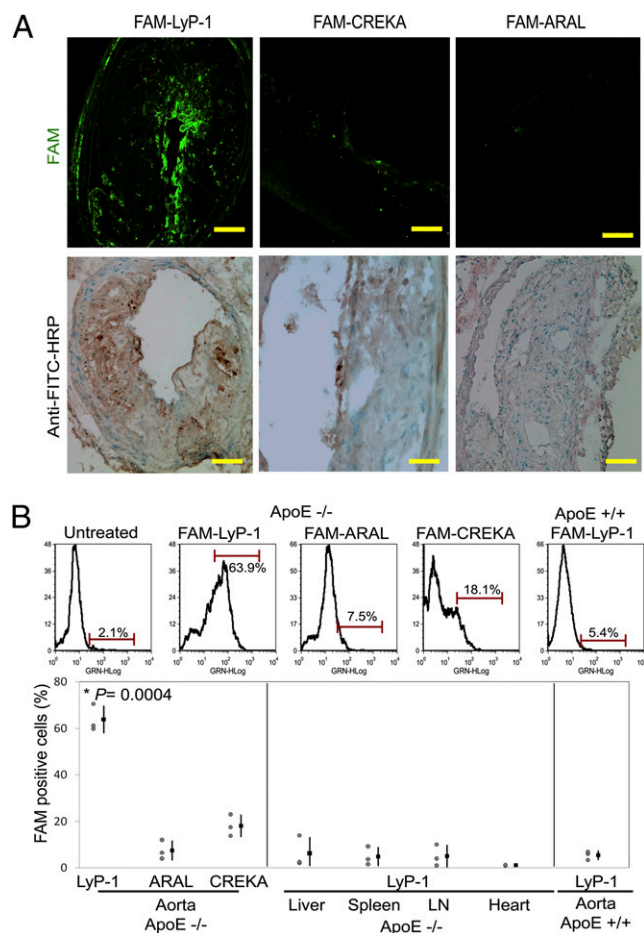


Fig. 1. Peptide homing to atherosclerotic plaques. Atherosclerotic mice were injected with 100 μ g of FAM-LyP-1 and the probe was allowed to circulate for 1 h, after which the aorta was collected and the peptide was detected in tissue sections by fluorescence detection and staining with anti-FITC-HRP antibodies (brown). (A) (Upper) A cross-section of aorta showing FAM-LyP-1 within plaque tissue. Only minimal fluorescence is observed in plaques from mice injected with FAM-CREKA and FAM-ARAL. (Lower) A representative image ($n = 5$ mice per group) of immunoperoxidase staining with an anti-FITC-HRP antibody showing LyP-1 accumulation in the plaque interior. (Original magnification, 20 \times .) (Scale bars, 100 μ m.) (B) Flow cytometry analysis of cells released from plaques. The histograms in the upper panels indicate the number of FAM-positive cells released from plaques after 4 h in vivo circulation. A high percentage of cells containing LyP-1 fluorescence is observed. The FAM-LyP-1 uptake by plaque cells was significantly greater than the uptake of CREKA, or the control peptide, ARAL; LyP-1 is not seen in the aorta of normal mice (ApoE^{+/+}). (* $P = 0.0004$ LyP-1 vs. FAM-CREKA, $n = 3$ mice per group).

plaques, CREKA (10). In agreement with the reported results, FAM-CREKA homed to the plaques in a pattern distinct from LyP-1 in that CREKA was essentially confined to the surface of the plaques (Fig. 1A). A control peptide, FAM-ARALPSQRSR (ARAL), did not accumulate in the plaques. FACS analysis of cells released from plaques (Fig. 1B) revealed elevated uptake of LyP-1 and CREKA relative to ARAL (percentage of FAM-positive cells; LyP-1, 63.9 \pm 5.8; CREKA, 18.1 \pm 4.6; ARAL, 7.5 \pm 4.1). LyP-1 accumulation was significantly higher than that of CREKA ($P < 0.0004$). There was no significant accumulation of LyP-1 in healthy aortas and nonaortic tissues of the atherosclerotic mice (Fig. 1B, and Figs. S1 and S2).

LyP-1 Targets Atherosclerotic Plaques. LyP-1 was initially identified as a homing peptide for tumor lymphatics (14, 15, 17). LyP-1

homing in tumors showed strong colocalization with the lymphatic markers, podoplanin and LYVE-1. Hence, we sought to determine whether lymphatic vessels in the plaques were a target for this peptide (14, 15, 17). Both plaque adventitia and intima were positive for podoplanin and LYVE-1 (Fig. S3). LyP-1 localized on the luminal surface of plaques (Fig. 2B, panel x) and within areas positive for podoplanin (Fig. 2B, panel y). The podoplanin staining in the interior of plaques showed no colocalization with blood vessel endothelia (CD31) or macrophages (CD11b and CD68) (Fig. 2A). A more widespread accumulation of LyP-1 in the plaque interior was observed in areas positive for macrophages, showing significant colocalization with these cells (Fig. 2C). Analysis of single cells released from plaques 4 h after intravenous LyP-1 injection (50% of which remained viable after tissue digestion) showed accumulation and internalization of the peptide in CD11b⁺ cells (Fig. 2D and Fig. S4). More than 60% of the total CD11b⁺ cells were positive for LyP-1 uptake (Fig. 2E) (P value = 0.0038 compared with CREKA and ARAL).

To understand the reasons for the affinity of LyP-1 for atherosclerotic plaques, we evaluated the expression of receptors associated with LyP-1 binding in plaques. Cell surface p32 protein has been shown to be the receptor in tumors that mediates the tumor homing of LyP-1 (14). In accordance with earlier results (16), we found p32 to be overexpressed in plaques (Fig. 3A). Immunostaining analysis of nonpermeabilized plaque sections and FACS quantification of cells released from plaques indicated p32 expression at the cell surface (Fig. 3B and C). In contrast, normal tissues, such as liver and spleen, showed no significant staining before permeabilization but were positive after permeabilization, indicating lack of cell surface localization of p32 (Fig. 3). Histological analysis performed on plaques also showed that p32 was highly expressed on macrophages, endothelia (Fig. S5, arrow x), and in areas that were also positive for podoplanin (Fig. S5, arrow y). LyP-1 homing colocalized with p32 staining inside plaques (Fig. 3D). Ex vivo analysis of peptide binding to primary cells released from plaques and to CD11b⁺ macrophages from 4T1-tumors known to express p32 on the cell surface showed significant binding of LyP-1 to these cells. In contrast, little binding of LyP-1 to normal cells, including monocytes/macrophages isolated from spleen and bone marrow cells, was observed (Fig. S6).

MRI of Plaque. Next, we examined the potential of LyP-1 as a targeting reagent to deliver nanoparticle-based imaging agents to plaques. Intravenously injected LyP-1-coated superparamagnetic iron oxide nanoworms (NWs) (18) accumulated in the interior of plaques (Fig. 4A). The NWs concentrated in cells expressing p32 and CD68 (Fig. S7). In comparison, the accumulation of untargeted NWs was low and limited to the luminal surface of plaques. CREKA-targeted NWs showed greater accumulation on the surface of the plaques, and minimally penetrated into the plaques, confirming reported results (10). Ex vivo MRI of aortas from mice injected with LyP-1-NWs revealed decreased T2*-weighted signal in areas that contained plaque (Fig. 4B). The axial images of the aorta facilitated a high-resolution comparison with optical imaging and immunohistochemistry, confirming that the NWs were present throughout the plaque volume and that nanoparticle distribution was significantly improved with LyP-1 targeting. Averaging of the T2*-weighted image amplitude throughout the aortic arch and descending aorta indicated that injection of LyP-1-conjugated NWs reduced the signal amplitude to a greater extent than CREKA-conjugated NWs (42% vs. 18%, $P < 0.01$).

MicroPET Imaging of 4-[¹⁸F]Fluorobenzoic Acid-Labeled LyP-1. We assessed the potential use of LyP-1 for PET imaging of atherosclerotic plaques. Dynamic imaging of intravenous injected [¹⁸F]FBA-LyP-1 over the first hour of circulation highlighted the aorta and the clearance tissues (kidneys and bladder). Radio-

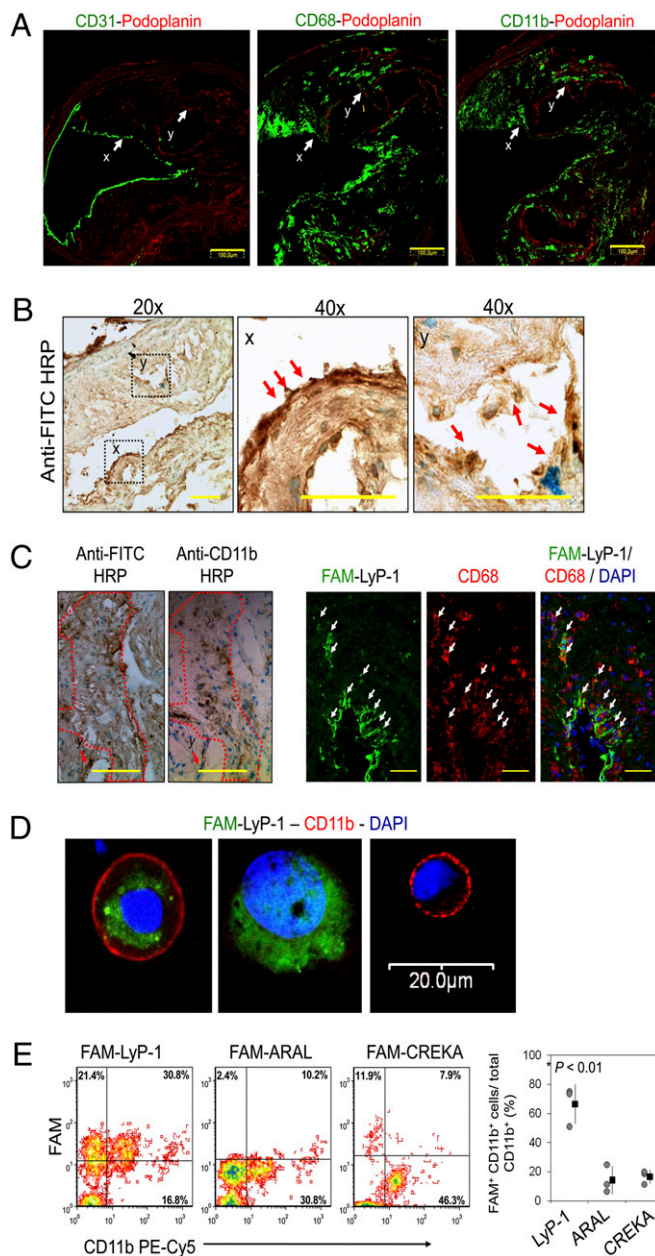


Fig. 2. LyP-1 accumulation in atherosclerotic plaques and association with the aortic endothelium, lymphatics, and macrophages. (A) Identification of the luminal endothelium (anti-CD31, green, x), lymphatics (anti-podoplanin, red, y) and macrophages (anti-CD68 or anti-CD11b, green) in aorta sections. (Original magnification 20 \times .) (Scale bars, 100 μ m.) (B) LyP-1 is seen at the luminal endothelium (arrow x) and in the lymphatics (arrow y). (Original magnification, 20 \times and 40 \times .) [Scale bars, 100 μ m (Left) and 50 μ m (Center, Right).] (C) LyP-1 accumulation in macrophage-rich areas in the plaque interior. (Right) FAM-LyP-1 localization in areas positive for the CD68 macrophage marker (red). The arrows point at cells expressing CD68 marker that were also positive for LyP-1 homing. (Original magnification, 40 \times .) [Scale bars, 100 μ m (Left) and 50 μ m (Right).] (D) Fluorescence microscopy analysis of cells released from plaque after 4 h of circulation. FAM-LyP-1 (green) is present in both CD11b⁺ (Left, red) and CD11b⁻ (Center) cells. Some CD11b⁺ cells do not contain LyP-1 (Right). (E) FACS analysis of the uptake of FAM-LyP-1, FAM-ARAL, and FAM-CREKA by CD11b⁺ plaque cells. More than half of the CD11b⁺ cells were positive for LyP-1 uptake, whereas CREKA was taken up by a small number of CD11b⁻ cells ($P = 0.0038$).

activity was also detected in the spine (Fig. 5). The LyP-1 signal detected in the spine was confirmed by histology analysis, but was much smaller than the accumulation in the plaques (Fig. S8).

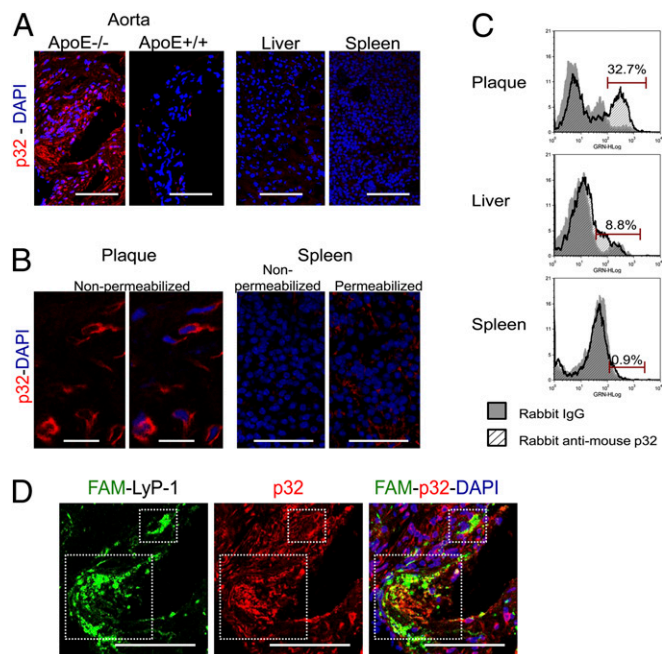


Fig. 3. Plaques express cell surface p32. (A) A representative confocal microscopy image showing that plaques are strongly positive for cell-surface p32 (ApoE^{-/-}; red), whereas normal aorta (ApoE^{+/+}) shows no staining. The blood vessels and parenchymal tissue of the major organs (shown for the liver and spleen) were also negative. (Original magnification, 40 \times .) (Scale bars, 50 μ m.) (B) Comparison of p32 staining in plaques and the spleen with and without permeabilization indicates cell surface p32 expression in the plaques, but not in the spleen. (Original magnification, 40 \times .) (Scale bars, 50 μ m.) (C) FACS histograms show that one third of cells released from plaques were positive for cell surface p32 expression, whereas there was only a minor shift of the fluorescence intensity when the liver and spleen cells were stained for p32. (D) Comparison of FAM-LyP-1 homing and p32 expression (red) indicates LyP-1 colocalizes in same region that expressed p32. Squares: regions where LyP-1 homing colocalized with p32 staining. (Original magnification, 20 \times .) (Scale bars, 100 μ m.)

Radioactivity in the reticulo-endothelial system was lower after the injection of [¹⁸F]FBA-LyP-1 compared with the control peptide [¹⁸F]FBA-ARAL (Fig. 5A) and several previously reported [¹⁸F]FBA-labeled peptides (19). Excised plaque-containing aortas from mice injected with [¹⁸F]FBA-LyP-1 showed a stronger PET signal throughout the aortic arch, roots, and descending aorta than normal aortas or plaque-containing aortas from mice injected with [¹⁸F]FBA-ARAL (Fig. 5A). The percentage of the injected dose per gram of tissue (% ID/g) in plaque-containing aortas of [¹⁸F]FBA-LyP-1-injected mice was fourfold higher after 3-h circulation (mean \pm SE; 0.31 \pm 0.05) than in aortas from normal mice injected with the same peptide (0.08 \pm 0.03; $P < 0.01$) and sixfold greater than in aortas from atherosclerotic mice injected with the control peptide (0.05 \pm 0.01; $P < 0.001$). Accumulation of [¹⁸F]FBA-LyP-1 was also significantly greater in plaque-containing aortas than in the heart, spleen, pancreas, and renal lymph nodes (<0.1% ID/g; $P < 0.01$) (Fig. 5A and Fig. S9). Although not statistically significant, the mean accumulation in plaque-containing aortas was also higher than in the blood (0.26% ID/g), the lungs (0.25% ID/g), and comparable to the liver (0.31% ID/g). Tissue biodistribution data confirmed that the kidneys were the main clearance organ for LyP-1 with mean accumulation of 1.95% ID/g.

Discussion

We report here plaque homing of a cyclic nonapeptide, LyP-1. The homing is specific; in accordance with earlier studies on the tumor-homing properties of LyP-1 (15, 17), this peptide showed

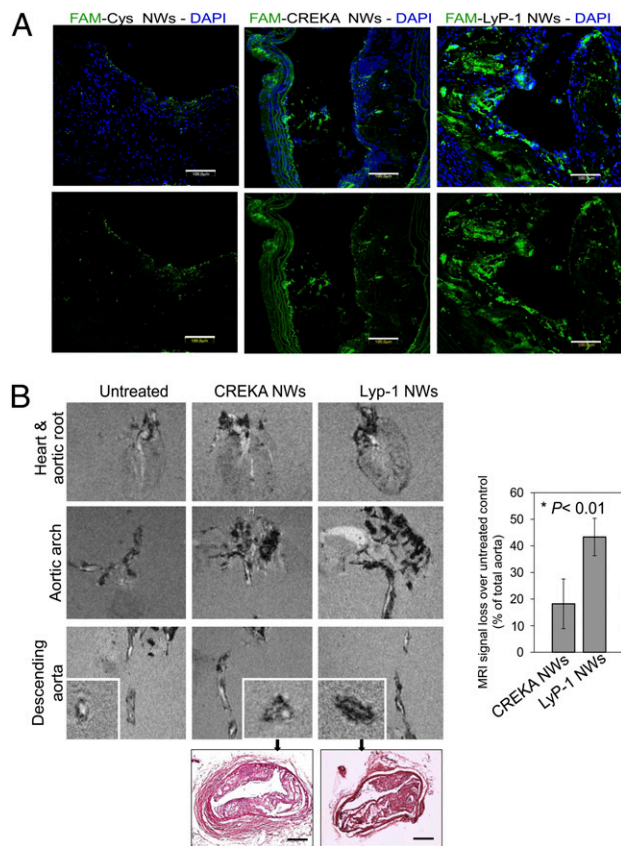


Fig. 4. LyP-1 targeted NWs home to the interior of plaques. FAM-LyP-1 and FAM-CREKA NWs were intravenously (retro-orbital) injected in ApoE-null mice under isoflurane inhalation at a dose of 5 mg/kg body weight and allowed to circulate for 6 h. (A) Histological analysis (FAM) shows minimal binding of nontargeted control NWs to the surface of plaques, whereas CREKA-targeted NWs show more accumulation on surface of plaques, and LyP-1-targeted NWs accumulate in the plaque interior. (Original magnification, 20 \times .) (Scale bars, 100 μ m.) (B) Ex vivo MRI of plaque. Shown are representative images from untreated mice and mice injected with CREKA NWs and LyP-1-NWs ($n = 3$ –4 per group), depicting the heart, aortic root, aortic arch, and descending aorta in axial and coronal planes. The axial slices show large plaque burden comparable to the H&E histology of respective cross-sections of the aorta. (Scale bars, 200 μ m.) (Right) LyP-1 NWs show a 42% decrease in T2* image amplitude compared with the untreated aorta ($P < 0.01$ by Tukey's Comparison).

no accumulation in various normal tissues, including the normal aorta. All plaque-containing regions within the aorta, regardless of the plaque size and volume, were receptive to LyP-1 homing. Our analysis indicated that the luminal blood vessel endothelium, lymphatic vessels, and the plaque macrophages were the predominant components positive for LyP-1 accumulation. Importantly, more than 50% of plaque-derived macrophages, a key component of plaques, showed LyP-1 internalization.

A remarkable feature of the LyP-1 homing to atherosclerotic plaques is that circulating LyP-1 penetrates into and accumulates deep within plaque tissue. LyP-1 penetration into the plaque interior is a unique feature not seen with previously reported plaque homing peptides, which primarily bind to the luminal surface of plaques or to cells close to the luminal surface (5, 6, 8–11). An example of such peptides is the CREKA peptide in this study, which almost exclusively delivers its payload to the luminal surface of plaques.

LyP-1 homing shows strong colocalization with the lymphatic markers (podoplanin and LYVE-1) (14, 15, 17). We detected vessel-like structures positive for both of these markers in the

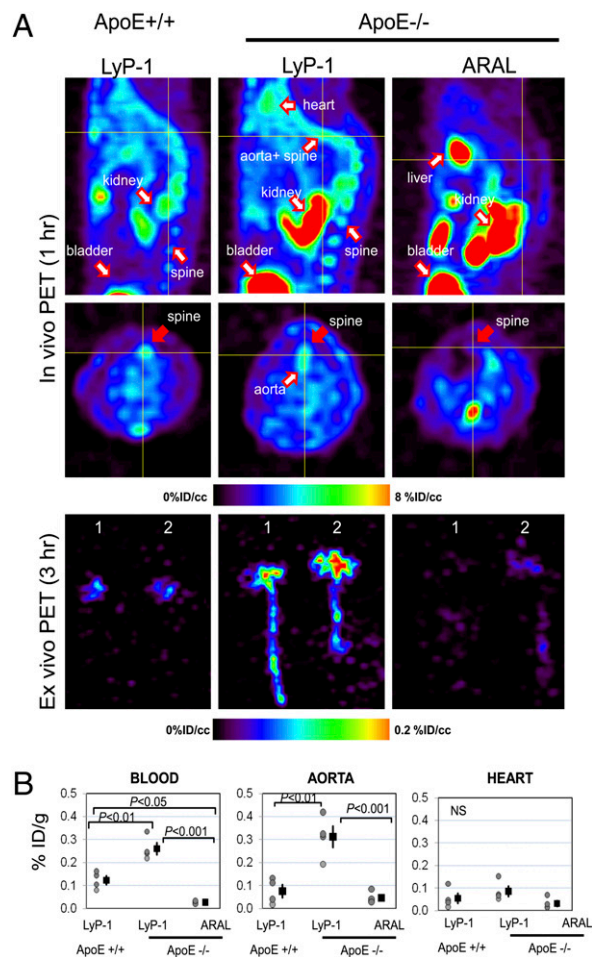


Fig. 5. MicroPET image and biodistribution analyses of atherosclerotic plaques targeted with LyP-1 labeled with [18 F]FBA. (A) Sagittal (Top) and transverse (Middle) maximum intensity projection in vivo PET images of [18 F]FBA radiotracer coupled to LyP-1 and control ARAL an hour after intravenous injection in wild-type ApoE $^{+/+}$ (for LyP-1 only) and in ApoE $^{-/-}$ (plaques) mice. The images showed overall tissue distribution (% ID/cc), of the peptide; distribution of [18 F]FBA-LyP-1 is detected within the aortic region, spinal region, and in clearance organs (kidneys and bladder) during 1-h circulation. Control peptide [18 F]FBA-ARAL shows widespread distribution in other organs. (Bottom) Maximum intensity projection images of ex vivo aortas indicate greater accumulation throughout the aortic arch, roots and descending region in aortas containing plaques after injection with radio-labeled LyP-1. (B) Biodistribution analysis of radioactivity (% ID/g) in blood, aorta, and heart after 3 h circulation. (Circle) Percentage of injected dose per gram from each mouse. (Square) mean percentage of injected dose per gram \pm SE for each group ($n = 4$ per group). Data show at least fourfold higher activity of [18 F]FBA-LyP-1 in aortas containing plaques than in the normal aortas and in [18 F]FBA-ARAL injected aortas ($P < 0.005$). [18 F]FBA-LyP-1 also has higher blood retention compared with [18 F]FBA-LyP-1 ($P < 0.005$), but limited traces in the heart (no significant difference in percentage of injected dose per gram of between the three groups).

plaque intima and even more abundantly in the plaque adventitia. Similar results have been published by others (20). The affinity of LyP-1 for lymphatics that are present in the plaques, and the absence of blood vessels in the plaque intima suggest that LyP-1 may enter plaque intima via the lymphatics.

LyP-1 also penetrates into tumor tissue (14, 15, 17). The tumor-penetrating properties of LyP-1 have been proposed to depend on what has been dubbed the “CendR” mechanism; after initial binding to tumor vessels, a tumor-homing peptide undergoes proteolytic processing to expose a cryptic CendR motif (R/KXXR/K),

the binding of which to neuropilin-1 triggers a transport pathway for extravasation and tissue penetration (21–23). LyP-1 contains a potential cryptic CendR motif (CGN**KRTR**GC; the bolded residues). Although the involvement of a CendR process in LyP-1 activity remains to be formally proven, it seems likely that this mechanism is responsible for the plaque and tumor penetration.

The LyP-1 receptor, p32, is expressed in the endothelial, smooth muscle, and inflammatory cells, such as the foam cells, of the plaque intima and media in human subjects (16). In this study, we found p32 to be highly expressed in the atherosclerotic plaques of apolipoprotein E (ApoE)-null mice maintained on a high-fat diet. Importantly, we found that p32 is present both on the cell surface and as an intracellular protein in the plaques. Tumor macrophages, and certain other cells in tumors, also express p32 at the cell surface, whereas in normal tissues, p32 is an intracellular (mitochondrial) protein, and not available to bind LyP-1 (this study and refs. 14, 24, and 25). Consequently, this high cell surface p32 expression, largely on (but not restricted to) plaque macrophages, confers LyP-1 its binding specificity for atherosclerotic plaques.

The role of p32 in disease is poorly understood, but it has been shown to be a critical regulator of the balance between oxidative phosphorylation and glycolysis in tumor cells (26). It has also been suggested that p32 interaction with its ligands may control the differentiation of inflammatory cells, such as macrophages and dendritic cells (27). Regardless of what its pathophysiological roles might be, it is clear that cell surface p32 expression and high LyP-1 binding are potentially useful markers for a class of inflammatory cells associated with atherosclerotic plaques and tumors.

We made use of the ability of LyP-1 to carry payloads to plaques in delivering PET and MRI contrast agents into plaque. It is noteworthy that the MRI imaging agent was a nanoparticle that is ~80-nm long and 30-nm wide, which, despite its large size, was effectively carried into the interior of the plaques by LyP-1. Iron oxide nanoparticles have previously been used for plaque imaging because they gradually accumulate in the plaque macrophages (2, 28). However, within the time frame we studied, we found no significant accumulation of nontargeted nanoparticles in plaques. In addition, a report by Briley-Saebo et al. (28) indicated that the intraplaque macrophage uptake of ~35-nm iron oxide particles is limited by the ability of the particles to traverse through the arterial endothelial wall. Our results show that providing the nanoparticles with a LyP-1 coating overcomes this obstacle. In addition, plaques contain cells other than macrophages that are positive for cell surface p32 expression and contribute to the accumulation of LyP-1 cargo in the plaques. The efficacy of the LyP-1-mediated plaque penetration was underscored by the difference in the localization of LyP-1 and CREKA; cargo bound to this previously identified plaque-homing peptide localized to the surface of plaques, but did not penetrate into the interior of the plaques (10).

We successfully imaged plaque with both MRI and PET in atherosclerotic mice. Ex vivo MRI imaging of the aortic root and the entire descending aorta showed that we can image LyP-1-targeted NWs in the entire aorta and throughout the plaque interior. In vivo imaging of iron oxide in mouse atherosclerosis has been shown to be feasible and to produce high-contrast images (e.g., refs. 29 and 30); however, the typical resolution of in vivo studies is >100 microns [e.g., 0.098 mm², and thus 313 μm in plane resolution (30)], which is not sufficient to differentiate the intraplaque distribution of LyP-1 and the plaque-surface accumulation of CREKA. In addition, PET imaging provided picomolar sensitivity in the imaging of monomeric LyP-1, quantifying the specific accumulation within aortic plaque. The retention of LyP-1 we encountered in the spine made it difficult to distinguish between the vascular signal and radioactivity in the spine in the sagittal images, but the two were clearly distinguished in the transverse images. There was a significant difference in the

signal density from the plaques and the spine in the immunohistochemistry assay of samples collected later, suggesting appropriate timing of the imaging could eliminate the interference from the spinal signal.

The higher avidity of multivalent LyP-1 constructs could further improve the efficacy of LyP-1-directed PET imaging. Although the resolution obtained with PET imaging (~1 mm) is substantially less than that obtained with high-field MRI (tens of microns), the exquisite sensitivity in tracking small constructs and the ability to rapidly survey vasculature for small disease foci are advantages with PET molecular imaging. Multimodal probes will also facilitate future combinations of PET and MRI, in which lesions are detected with PET and mapped at high resolution with MRI (31).

In conclusion, the LyP-1 peptide shows specific homing to atherosclerotic plaques and penetrates into the interior of the plaques, taking with it payloads ranging in size from small molecules to nanoparticles. Applications in diagnostic imaging, in the assessment of response to therapy, and in the delivery of therapeutic compounds into plaques are envisioned.

Materials and Methods

Peptide Synthesis. Peptides were synthesized as previously described (23) using an automatic microwave-assisted peptide synthesizer (Liberty; CEM Corp.) and purified to greater than 90% purity. The synthesis of LyP-1 with an extra N-terminal cysteine used for the chemoselective ligation will be described elsewhere.

Preparation of Iron Oxide Nanoworms. Peptide-coated iron-oxide NWs (32) were prepared as previously described (18). The NWs were about 80 to 110 nm in length and 30 nm in width. The blood half-life of the LyP-1 NW was 12 h.

Radiochemistry. 4-[¹⁸F]Fluorobenzoic acid ([¹⁸F]FBA) was prepared using modifications from previously published reports (30, 33). The subsequent N-terminal solid phase radiolabeling of LyP-1 and ARAL with [¹⁸F]FBA was achieved following previously published methods (19). In brief, the cleaved [¹⁸F]FBA-LyP-1 and [¹⁸F]FBA-ARAL mixture were evaporated and the desired radiolabeled peptides were isolated by semipreparative RP-HPLC (Luna C18, 250 mm × 10 mm; Phenomenex). Radiochemical purity of isolated peptides on HPLC were more than 95% and specific activity was >20 GBq/mmol. The collected product was isolated in ethanol/acetic acid and formulated to physiological pH for injection.

Animal Protocols and in Vivo Administration of Reagents. Atherosclerotic plaques in male and female mice homozygous for the ApoE1Unc mutation (ApoE-null mice) (The Jackson Laboratory) were induced by maintaining the mice on a high-fat diet (34, 35) for 6 to 8 mo. Healthy aortas were obtained from age-matched C7BL/6 wild-type mice fed on a normal diet. The mice were housed and all procedures performed with the approval and according to standards of the University of California, Santa Barbara and University of California, Davis Institutional Animal Care and Use Committees. To test peptide homing, the mice were injected retro-orbitally under isoflurane inhalation (isoflurane 2–3% vol/vol + 2 L/min O₂) anesthesia and, when applicable, subsequently perfused with high-glucose DMEM and PBS through the left ventricle to remove unbound reagent. Tissues were excised and left unfixed or fixed with 4% paraformaldehyde.

Immunohistochemistry and Antibodies. Fresh-frozen OCT-embedded tissue was sectioned at 7 μm, fixed with ice-cold acetone, blocked with 4% serum in PBS, and stained with antibodies. The following antibodies were used: anti-mouse p32 [rabbit polyclonal (14)], CD68 (rat monoclonal; eBioscience), CD11b (rat monoclonal; eBioscience), CD31 (rat monoclonal; eBioscience), podoplanin (hamster monoclonal; eBioscience), LYVE-1 (rat monoclonal; eBioscience), anti-FITC-HRP (goat polyclonal; ACRIS Antibodies). Purified rat IgG2a κ isotype control (BD Pharmingen), normal rabbit IgG (R&D) and normal goat IgG (R&D) were used as controls. The following secondary antibodies from Invitrogen were used for detection: goat anti-rat 488/546, goat anti-rabbit 488/546, donkey anti-goat 488/546, goat anti-hamster 546, and goat anti-rat 647. Primary antibodies were incubated for 1 to 4 h at room temperature, or at 4 °C to detect cell surface expression. Stained tissue sections were mounted in Vectashield DAPI-containing mounting media (Vector Laboratory). Immunoperoxidase staining with anti-FITC-HRP was

performed using DAB (MP Biomedicals) reaction and the sections were counter stained with 1% methyl green (Sigma Aldrich).

Microscopy and Imaging Analyses. Tissue sections were examined under a FluoView 500 confocal laser-scanning microscope (Olympus) or BX60 fluorescence microscope with MiroFire camera (Olympus). Whole-tissue uptake of fluorescein-labeled peptides following in vivo circulation was imaged using a 530-nm viewing filter, Illumatool light source (Light Tools Research) and recorded with a Canon XTi DSLR camera.

Flow Cytometry. Cells from plaques and other tissues were released into suspension by 2-h incubation at 37 °C in a tissue digestion mixture containing 450 U/mL collagenase type 1 (Worthington Biochemical), 1 mg/mL soybean trypsin inhibitor (Worthington Biochemical), 4.7 U/mL elastase (Worthington Biochemical), 1 mg/mL DNase 1 (Sigma Aldrich), and 0.5% FCS. CD11b PE-Cy5 (rat monoclonal; eBioscience) was used to identify monocytes/macrophages. Positive cells were quantified on GUAVA FACS instrument (Millipore) and data were analyzed using FCS Express Version 3 (De Novo Software).

MR Imaging and Analysis. Excised tissues from $n = 3$ to 4 mice per group were fixed in 4% PFA for 48 h and embedded in 3% agarose in PBS. The gel-embedded tissues were subjected to T2*-weighted MRI scans with a 7T MR imager (Bruker Biospin) using a FLASH sequence with flip angle of 30°, repetition time/echo time of 1,000/15 ms, 512×512 acquisition, 290- μ m slice thickness, and 2.9 by 2.9-cm regions of interest extending over the heart, aortic arch, and descending aorta. Images were processed in ImageJ software, where regions of interest were drawn within the aortic wall of each image and the signal amplitude recorded and averaged after histogram correction for small variations in image amplitude. After imaging, tissues were sectioned for histological analysis with H&E staining.

MicroPET Imaging and Biodistribution. A total of eight male and female ApoE-null mice on high fat diet (>6 mo) and four female C57BL/6 wild-type mice were used for microPET imaging. Anesthetized animals with 2% to 3% isoflurane were placed in pairs on the scanner bed and PET acquisitions were obtained as described (19) using a dedicated small-animal PET scanner (Focus120; Siemens Medical Solutions, Inc.). In vivo PET scans were obtained for 1 h immediately after tail vein injection of ~ 150 μ Ci of the radio-labeled peptides in 150 μ L PBS and for 30 min at 3 h after injection. Ex vivo excised aortas attached to the heart were imaged for 30 min (3 h after injection). Acquired 1-h histograms were reconstructed to four dynamic images (15-min intervals) with maximum a posterior estimation. The biodistribution of radioactivity in collected organs was measured in a γ -counter (Perkin-Elmer Life Sciences).

Statistical Analysis. Mean differences between groups were statistically tested using two-tailed Student's unpaired t test or one-way ANOVA followed by a suitable post hoc test. A P value of less than 0.05 was considered statistically significant.

Note Added in Proof. An article showing the homing of LyP-1-coated nanoparticles to atherosclerotic plaques recently appeared on line (36). To the extent the data in the two papers overlap, they are in full agreement.

ACKNOWLEDGMENTS. We thank Brett Z. Fite for help with MRI acquisition, Heather Lindfors for the synthesis of imaging probes, Julie Beegle for PET scanning, and Dr. Eva Engvall for comments on the manuscript. This work was supported by National Heart, Lung, and Blood Institute Program of Excellence in Nanotechnology Grant HL070818 and, in part, by Grant W81XWH-08-1-0727 from the Department of Defense (to E.R.), National Heart, Lung, and Blood Institute Contract no. HHSN268201000043 (to K.W.F.), and an American Heart Association Post-doctoral Fellowship (to J.H.).

- Ruoslahti E, Bhatia SN, Sailor MJ (2010) Targeting of drugs and nanoparticles to tumors. *J Cell Biol* 188:759–768.
- Nahrendorf M, et al. (2008) Nanoparticle PET-CT imaging of macrophages in inflammatory atherosclerosis. *Circulation* 117:379–387.
- Jaffer FA, et al. (2008) Real-time catheter molecular sensing of inflammation in proteolytically active atherosclerosis. *Circulation* 118:1802–1809.
- Pasqualini R, Ruoslahti E (1996) Organ targeting in vivo using phage display peptide libraries. *Nature* 380:364–366.
- Kelly KA, Nahrendorf M, Yu AM, Reynolds F, Weissleder R (2006) In vivo phage display selection yields atherosclerotic plaque targeted peptides for imaging. *Mol Imaging Biol* 8:201–207.
- Nahrendorf M, et al. (2006) Noninvasive vascular cell adhesion molecule-1 imaging identifies inflammatory activation of cells in atherosclerosis. *Circulation* 114:1504–1511.
- Nahrendorf M, et al. (2009) 18F-4V for PET-CT imaging of VCAM-1 expression in atherosclerosis. *JACC Cardiovasc Imaging* 2:1213–1222.
- Liu C, Bhattacharjee G, Boisvert W, Dilley R, Edgington T (2003) In vivo interrogation of the molecular display of atherosclerotic lesion surfaces. *Am J Pathol* 163:1859–1871.
- Nicol CG, et al. (2009) Use of in vivo phage display to engineer novel adenoviruses for targeted delivery to the cardiac vasculature. *FEBS Lett* 583:2100–2107.
- Peters D, et al. (2009) Targeting atherosclerosis by using modular, multifunctional micelles. *Proc Natl Acad Sci USA* 106:9815–9819.
- Hong HY, et al. (2008) Phage display selection of peptides that home to atherosclerotic plaques: IL-4 receptor as a candidate target in atherosclerosis. *J Cell Mol Med* 12(5B):2003–2014.
- Simberg D, et al. (2007) Biomimetic amplification of nanoparticle homing to tumors. *Proc Natl Acad Sci USA* 104:932–936.
- Wilson HM, Barker RN, Erwig LP (2009) Macrophages: Promising targets for the treatment of atherosclerosis. *Curr Vasc Pharmacol* 7:234–243.
- Fogal V, Zhang L, Krajewski S, Ruoslahti E (2008) Mitochondrial/cell-surface protein p32/gC1qR as a molecular target in tumor cells and tumor stroma. *Cancer Res* 68:7210–7218.
- Laakkonen P, Porkka K, Hoffman JA, Ruoslahti E (2002) A tumor-homing peptide with a targeting specificity related to lymphatic vessels. *Nat Med* 8:751–755.
- Peerschke EI, et al. (2004) Expression of gC1q-R/p33 and its major ligands in human atherosclerotic lesions. *Mol Immunol* 41:759–766.
- Laakkonen P, et al. (2004) Antitumor activity of a homing peptide that targets tumor lymphatics and tumor cells. *Proc Natl Acad Sci USA* 101:9381–9386.
- Agemy L, et al. (2010) Nanoparticle-induced vascular blockade in human prostate cancer. *Blood* 116:2847–2856.
- Gagnon MK, et al. (2009) High-throughput in vivo screening of targeted molecular imaging agents. *Proc Natl Acad Sci USA* 106:17904–17909.
- Nakano T, et al. (2005) Angiogenesis and lymphangiogenesis and expression of lymphangiogenic factors in the atherosclerotic intima of human coronary arteries. *Hum Pathol* 36:330–340.
- Teesalu T, Sugahara KN, Kotamraju VR, Ruoslahti E (2009) C-end rule peptides mediate neuropilin-1-dependent cell, vascular, and tissue penetration. *Proc Natl Acad Sci USA* 106:16157–16162.
- Sugahara KN, et al. (2010) Coadministration of a tumor-penetrating peptide enhances the efficacy of cancer drugs. *Science* 328:1031–1035.
- Sugahara KN, et al. (2009) Tissue-penetrating delivery of compounds and nanoparticles into tumors. *Cancer Cell* 16:510–520.
- Muta T, Kang D, Kitajima S, Fujiwara T, Hamasaki N (1997) p32 protein, a splicing factor 2-associated protein, is localized in mitochondrial matrix and is functionally important in maintaining oxidative phosphorylation. *J Biol Chem* 272:24363–24370.
- Dedio J, Jahnen-Dechent W, Bachmann M, Müller-Esterl W (1998) The multiligand-binding protein gC1qR, putative C1q receptor, is a mitochondrial protein. *J Immunol* 160:3534–3542.
- Fogal V, et al. (2010) Mitochondrial p32 protein is a critical regulator of tumor metabolism via maintenance of oxidative phosphorylation. *Mol Cell Biol* 30:1303–1318.
- Hosszu KK, Santiago-Schwarz F, Peerschke EI, Ghebrehiwet B (2010) Evidence that a C1q/C1qR system regulates monocyte-derived dendritic cell differentiation at the interface of innate and acquired immunity. *Innate Immun* 16:115–127.
- Briley-Saebo KC, et al. (2011) Targeted iron oxide particles for in vivo magnetic resonance detection of atherosclerotic lesions with antibodies directed to oxidation-specific epitopes. *J Am Coll Cardiol* 57:337–347.
- Morris JB, et al. (2008) p38 MAPK inhibition reduces aortic ultrasmall superparamagnetic iron oxide uptake in a mouse model of atherosclerosis: MRI assessment. *Arterioscler Thromb Vasc Biol* 28:265–271.
- Guhlke S, Wester HJ, Bruns C, Stöcklin G (1994) (2-[18F]fluoropropionyl-(D)phe1)-octeotide, a potential radiopharmaceutical for quantitative somatostatin receptor imaging with PET: Synthesis, radiolabeling, in vitro validation and biodistribution in mice. *Nucl Med Biol* 21:819–825.
- Jarrett BR, Correa C, Ma KL, Louie AY (2010) In vivo mapping of vascular inflammation using multimodal imaging. *PLoS ONE* 5:e13254.
- Park JH, et al. (2010) Cooperative nanomaterial system to sensitize, target, and treat tumors. *Proc Natl Acad Sci USA* 107:981–986.
- Sutcliffe-Goulden JL, et al. (2002) Rapid solid phase synthesis and biodistribution of 18F-labelled linear peptides. *Eur J Nucl Med Mol Imaging* 29:754–759.
- Reddick RL, Zhang SH, Maeda N (1994) Atherosclerosis in mice lacking apo E. Evaluation of lesional development and progression. *Arterioscler Thromb* 14:141–147.
- Maeda N, et al. (2007) Anatomical differences and atherosclerosis in apolipoprotein E-deficient mice with 129/SvEv and C57BL/6 genetic backgrounds. *Atherosclerosis* 195:75–82.
- Uchida M, et al. (2011) Protein cage nanoparticles bearing the LyP-1 peptide for enhanced imaging of macrophage-rich vascular lesions. *ACS Nano*, in press.